INFLUENCE OF MATERIAL VELOCITY ON HEAT GENERATION DURING LINEAR WELDING STAGE OF FRICTION STIR WELDING

by

Alin MURARIU [a], ***Darko M. VELJIĆ*** [b*], ***Dragana R. BARJAKTAREVIĆ*** [c], ***Marko P. RAKIN*** [c], ***Nenad A. RADOVIĆ*** [c], ***Aleksandar S. SEDMAK*** [d], ***and Jelena M. DJOKOVIĆ*** [e]

[a] ISIM, Timisoara, Romania
[b] IHIS Science & Technology Park, IHIS Techno Experts R&D Center, Belgrade, Serbia
[c] Faculty of Technology and Metallurgy, University of Belgrade, Serbia
[d] Faculty of Mechanical Engineering, University of Belgrade, Serbia
[e] Technical Faculty in Bor, University of Belgrade, Serbia

Original scientific paper
DOI:10.2298/TSCI150904217M

The heat generated during friction stir welding process depends on plastic deformation of the material and friction between the tool and the material. In this work, heat generation is analysed with respect to the material velocity around the tool in Al alloy Al2024-T351 plate. The slip rate of the tool relative to the workpiece material is related to the frictional heat generated. The material velocity, on the other hand, is related to the heat generated by plastic deformation. During the welding process, the slippage is the most pronounced on the front part of the tool shoulder. Also, it is higher on the retreating side than on the advancing side. Slip rate in the zone around the tool pin has very low values, almost negligible. In this zone, the heat generation from friction is very low, because the material is in paste-like state and subjected to intensive plastic deformation. The material flow velocity around the pin is higher in the zone around the root of the pin. In the radial direction, this quantity increases from the pin to the periphery of the tool shoulder.

Key words: *friction stir welding, numerical simulation, material velocity, slip rate, heat generation, equivalent plastic strain*

Introduction

Friction-stir welding (FSW) is a modern welding process which can be used for joining different materials and their combinations: aluminum and its alloys, copper and its alloys, magnesium, zinc, titanium and its alloys, mild steel, *etc*. There are two main stages of FSW-plunging of the tool into the material (plunge stage) and welding stage (often called linear welding stage). During the plunge stage, the welding tool, fabricated from much stronger and harder material, penetrates into the plates positioned for welding. FSW process has been previously considered in the literature [1-15], from the point of view of manufacturing, modelling, as well as testing of the specimens cut from the welded joints. In the papers [3, 4], numerical modelling of the plunge stage and linear welding stage is presented by the authors. In the paper [5], the authors have analysed the heat generation during the plunge stage of FSW; this is important because the thermo-mechanical conditions which exist during the linear welding stage

* Corresponding author; e-mail: veljic.darko@gmail.com

are initiated during the plunge stage. Heat generation is also considered in some other studies, using experimental [10] or numerical [12] examination.

During the linear welding stage of FSW, the energy is generated by two processes: friction between the tool and welded material, and intensive plastic deformation of the material. Both of these energy components (which summed give total energy) heat the plates which are being welded, and the joint is accomplished at temperature values below the melting point. In the early welding stage, the amount of generated heat is not balanced with the dissipated heat; this balance is established later during the linear welding stage. Having in mind the movement of the tool, *i. e*. rotation and translation, the friction between the welded material and the tool depends on the slip rate – relative velocity of the tool with respect to the material. The relevant tool velocity is circumferential velocity, which depends on the rotation angular velocity and distance from the rotation axis. The material is also in motion, and this is expressed through material velocity – of course, this quantity is related to plastic deformation, and therefore influences the heat generation due to plastic deformation. Slip rate at a certain contact point is therefore obtained as the difference between the circumferential velocities of the tool and material at that point.

This paper deals with the heat generation during FSW of aluminum alloy Al2024-T351; both amount and rate of heat generation have been considered. Having in mind that the friction at the contact surfaces of the tool and the plates is a consequence of the relative movement, analysis of their velocities reveals valuable data about this contact interaction. First of all, distribution of slip rate at the contact surfaces is tracked, in order to determine the friction intensity. On the other hand, material flow velocities are analysed due to their influence on plastic deformation.

Material

Chemical composition of 2024-T351 aluminum is as follows: aluminum (Al)-Balance, Cu-4.52, Mg-1.60, Mn-0.65, Fe-0.28, Si-0.12, Zn-0.09, Ti-0.16, Cr-0.01, other, total-0.02% [16]. Other properties of this alloy are given in tabs. 1 and 2.

Table 1. Tensile properties of aluminum alloy 2024 T351 [16]

0.2% yield strength $R_{p0.2}$ [MPa]	Tensile strength R_m [MPa]	Elongation at fracture A_5 [%]
324	469	20

Table 2. Material properties of aluminum alloy 2024 T351 [4, 16, 17]

Material properties	Value
Young's modulus of elasticity [GPa]	73.1
Poisson´s ratio [–]	0.33
Thermal conductivity [$Wm^{-1}°C^{-1}$]	121
Coefficient of thermal expansion [$°C^{-1}$]	$24.7 \cdot 10^{-6}$
Density [kgm^{-3}]	2770
Specific heat capacity [$Jkg^{-1}°C^{-1}$]	875
Solidus, liquidus [°C]	502, 638

Finite element model

Numerical simulations could be applied in development and optimization of any welding process, as given in papers [18-20]. In addition to the simulation of the process itself, numerical methods are also applied in determining the residual stresses in the joints [21], as well as in fracture assessment of the welded structures, [15, 22]. The finite element model (FE) of the plates (100 × 50 × 3 mm), used in this paper, is shown in fig. 1. The model is formed using hexahedral 8-noded elements, with trilinear displacement and temperature degrees of freedom according to [23]. This element, denoted in Abaqus software package as C3D8RT, has uniform strain and hourglass control [12, 13, 23]. The model consists of 32298 nodes and 28522 elements. The

welding tool (fig. 2) and the backing plate are considered as rigid bodies in the numerical model. Therefore, the tool and plate have only 6 mechanical degrees of freedom for the entire body, and no thermal degrees of freedom at all. Plunge depth of the welding tool shoulder is 0.2 mm. The geometry of the tool is simplified, which means that the thread is not modelled,

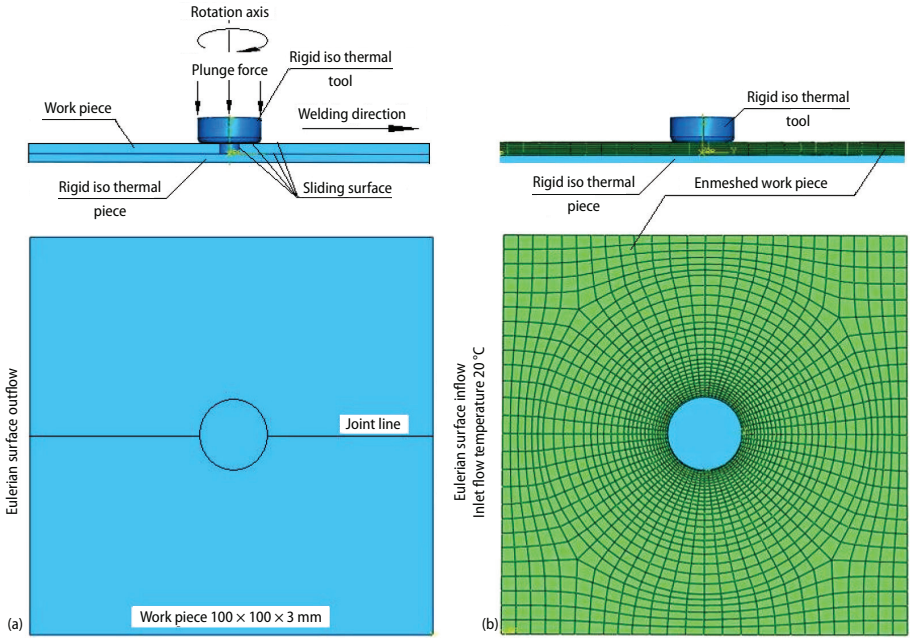

Figure 1. The FE model (a) and mesh (b) of the welding plates, tool and backing plate

as it is shown in fig. 2. Such approach is applied because the thread might lead to excessive mesh distortion in the plate.

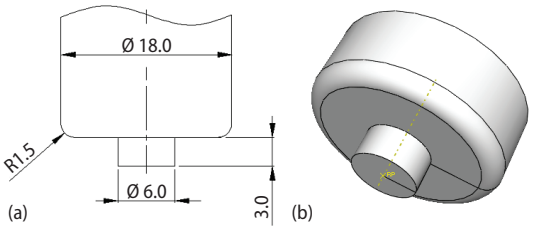

Figure 2. The welding tool model (rigid body)

Thermal analysis

In Abaqus/Explicit, the heat transfer equations are integrated using the explicit forward-difference time integration rule [23]:

$$T_{i+1}^{\mathrm{N}} = \Delta t_{i+1}\dot{T}_i^{\mathrm{N}} + T_i^{\mathrm{N}} \tag{1}$$

where T^{N} is the temperature at node N and the subscript i refers to the increment number in an explicit dynamic step.

The value of the heat transfer coefficient at the bottom surface of the workpiece is 3000 W/m^2°C, [2, 14]; this value corresponds to the heat transfer through the backing plate. Heat convection coefficient on the other surfaces of the workpiece is h = 10 W/m^2°C [12, 14]. These surfaces are in the contact with the ambient (air), with the ambient temperature 25 ºC.

Friction interaction between the welding tool and the material is characterised by the value of friction coefficient 0.3.

Mechanical analysis

The equation for mechanical response of the material is [23]:

$$p = \rho\vec{u} + k\vec{u} \tag{2}$$

where ρ is the density, k – the stiffness coefficient, p – the body force and $\vec{u}$ – the displacement vector.

Johnson-Cook material law, which is used to model the dependence of yield stress on strain rate and temperature, is given by [24]:

$$\sigma_y = \left[A + B(\varepsilon_p)^n\right]\left[1 + C\left(\frac{\dot{\varepsilon}_p}{\dot{\varepsilon}_o}\right)\right]\left[1 - \left(\frac{T - T_{room}}{T_{melt} - T_{room}}\right)^m\right] \tag{3}$$

where T_{melt} = 502 °C is the melting point or solidus temperature, T_{room} = 20 °C – the ambient temperature, T [°C] – the effective temperature, A = 265 MPa – the yield stress, B = 426 MPa – the strain factor, n = 0.34 – the strain exponent, m = 1 – the temperature exponent, and C = 0.015 – the strain rate factor. *A, B, C, n, T_{melt}, T_{room}* and *m* are material constants for the Johnson-Cook law for the examined alloy Al 2024 T351 [24, 25].

Results and discussion

Figure 3 shows the field of the slip rate after 2 and 10 s; this is actually relative velocity of the tool with respect to the plates being welded. At the end of the tool plunge, relative velocity is the highest at the periphery of the contact between the tool and material, because this is the region with less intensive heating of the material, while circumferential velocity of the tool is the highest. The field of this quantity (slip rate) is still approximately symmetrical with respect to the welding tool axis after 2 s (left-hand side of fig. 3). After 10 s, the slippage is the most intensive at the front part of the tool shoulder, on the advancing side. This can be

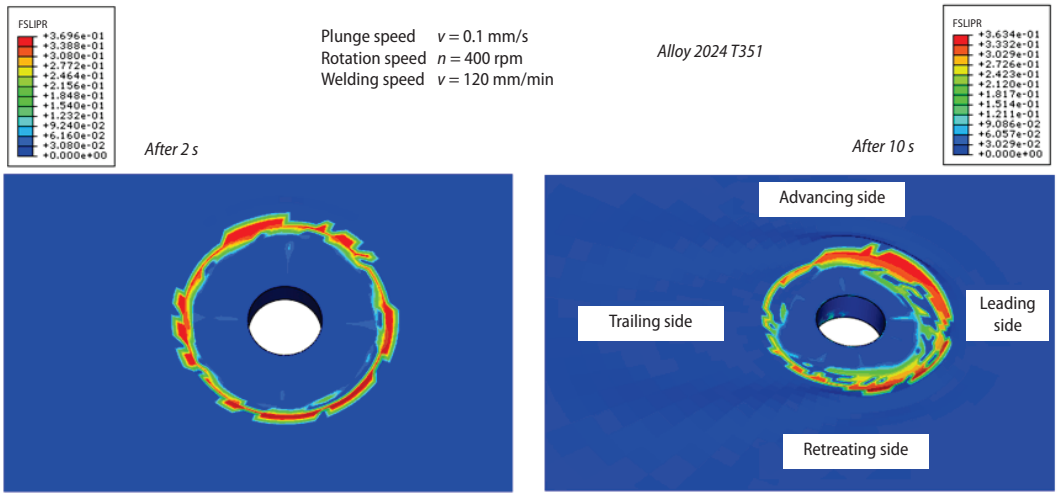

Figure 3. Relative movement of the tool with respect to the material – slip rate $\dot{\gamma}$ after 2 and 10 seconds

seen through high slip rate values in the right-hand side of fig. 3 (highest values are located on the quarter of the shoulder circumference between the leading and advancing side). This is expected, because the tool shoulder on its front side comes into contact with the "new" material, which is less heated in comparison with the material under the shoulder. Therefore, sticking of the material to the welding tool is less intensive. Having in mind that the contact pressure is higher in this zone, the friction will also be more intensive. Slip rate in the zone around the tool pin is significantly lower. The amount of friction-generated heat is much lower in this zone, because the material is in a paste-like state and is exposed to intensive plastic deformation.

Figures 4 and 5 show the vectors of the material flow velocity, while fig. 6 gives the distribution of this velocity around the tool pin and under the tool shoulder. At the end of the tool plunge, the material flow velocity around the pin is almost uniform along the entire height (of the pin), and the material flow velocity under the shoulder increases linearly with the radius, left-hand side of fig. 6. During the welding process, it can be seen that the material flow rate around the pin in the root of the pin (under the tool shoulder) is higher in comparison with the values near the tip of the pin. Actually, contact pressure in the zone of the root is higher than near the tip. This also results in higher contact stresses, because the tool shoulder presses the material downwards. This leads to sticking of the material to the tool in the root zone, *i. e.* plastic deformation is more pronounced and material movement is faster. In comparison with the material flow at the advancing side, the material flow is faster at the retreating side. Lower velocities in the root of the pin at the advancing side can clearly be seen in fig. 5 (as shorter arrows). For a good quality of the welded joint, the material has to have a good flow from the

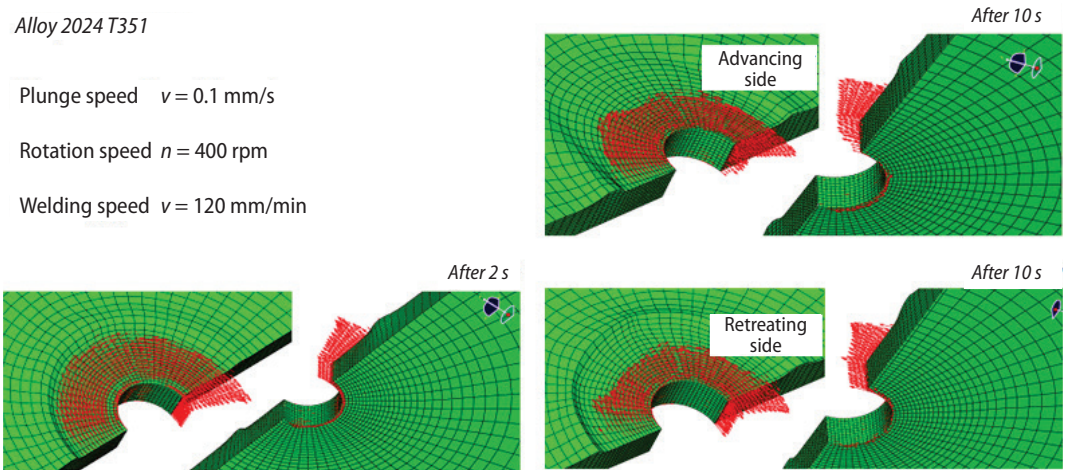

Figure 4. Vector display of the material flow velocity around the tool pin and shoulder on the advancing and retreating side (*for color image see journal web site*)

retreating to the advancing side; otherwise, if the quantity of the material brought to the advancing side is insufficient, errors in the form of tunnelling can occur.

In fig. 7a, the amount of heat generated by plastic deformation and friction is shown, along with their sum - total heat. Figure 7b presents the corresponding heat generation rates. In the beginning of the plunge of the tool shoulder, friction-generated heat is dominant. When a certain temperature is reached, i.e. when the material in the contact zone becomes soft enough, the conditions for sticking the material to the tool are reached. A large percentage of the contact

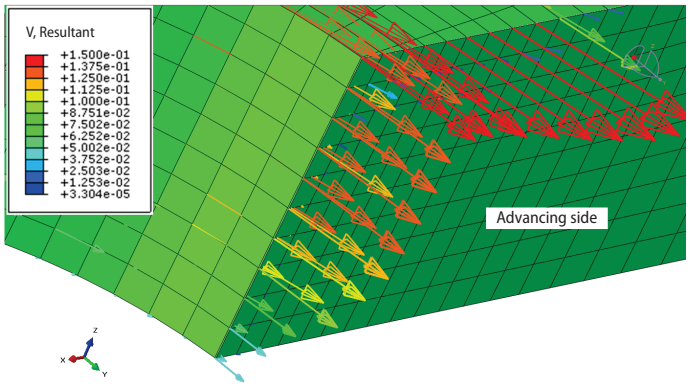

Figure 5. Vector display of the material flow velocity around the tool pin and shoulder – detailed view of the advancing side after 10 s (*for color image see journal web site*)

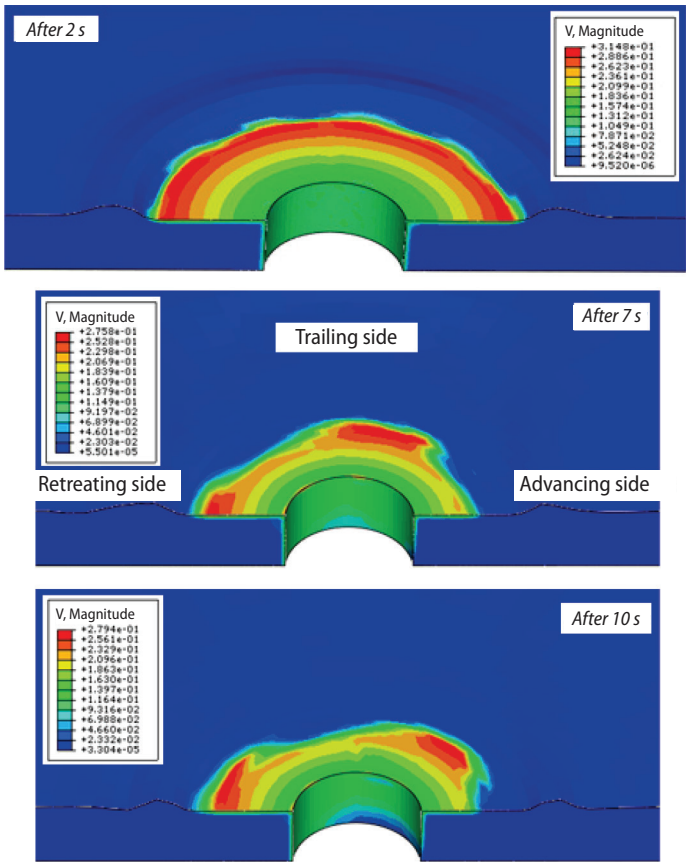

Figure 6. Distribution of material flow velocities around the tool pin and shoulder after 2, 7, and 10 seconds
(*for color image see journal web site*)

surface is in motion (fig. 6), so the friction heat generation rate suddenly decreases. Temperature on the contact surface which corresponds to this state cannot exceed 502 ºC, because the material loses the plastic deformation resistance; this is reflected in the expression for the Johnson-Cooke material law, eq. (3). Therefore, in addition to sudden decrease of heat generation rate due to friction, a gradual decrease of heat generation rate due to plastic deformation begins.

The rate of total heat generation has reached the maximum value 3.4 kJ/s, due to the high percentage of the friction-generated heat. After 2 s, when the linear welding stage begins, the rate of total heat generation has decreased to 1.9 kJ/s, and after 9 s (when the welding regime became stationary), it is almost constant at the level around 1.3 kJ/s.

From this diagram, it can be concluded that the amount of the friction-generated heat is also higher than the amount of heat generated by plastic deformation after the process is stabilised. The relative portion of friction-generated heat is around 60% of the total generated heat, while the remaining 40% comes from plastic deformation. In the stationary regime (after 9-10 seconds), it can be regarded that the amount of generated heat is equal to amount of dissipated heat.

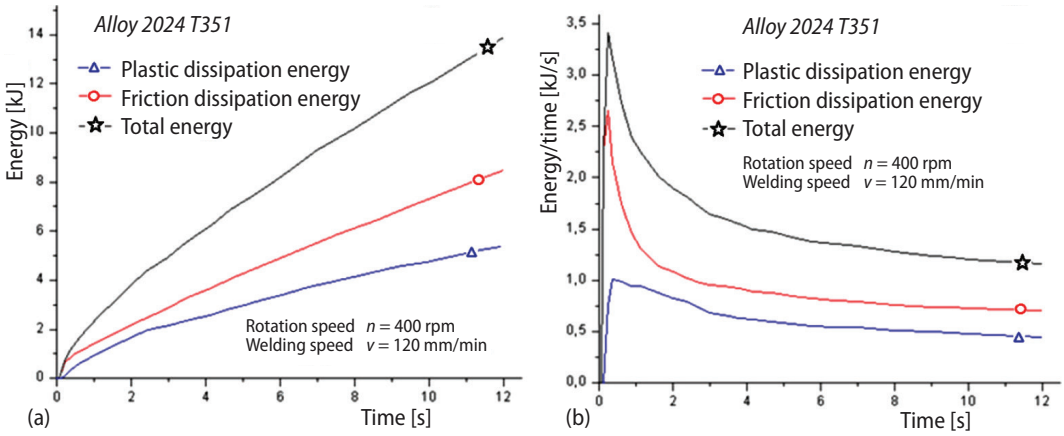

Figure 7. Heat generation during linear welding: energy (a) and energy rate (b)

Conclusions

For good quality of the welded joint, it is necessary that the material has good flow from the retreating toward the advancing side; otherwise, if the quantity of the material brought to the advancing side, errors like tunnelling can occur. The slip rate is related to the friction-generated heat, while the velocity of the material is related to the heat generated by the plastic deformation. From the presented results, the following conclusions can be drawn.

- At the end of the tool plunging, the slip rate is the highest at the periphery of the tool – plate contact, because the material in this region is less intensively heated, and circumferential velocity of the tool is the highest.
- During the welding, slippage is the most intensive at the front of the shoulder, at the advancing side. The tool shoulder on its front side comes into contact with the "new" material, which is less heated in comparison with the material under the shoulder – the sticking of the material to the tool is less intensive.
- Slip rate in the zone around the tool pin is significantly lower. The amount of friction-generated heat is much lower in this zone, because the material is in a paste-like state and is exposed to intensive plastic deformation.
- The velocity of the material increases from the tool pin to the periphery of the tool shoulder; this increase is approximately linear during the tool plunging and in the beginning of the welding stage.
- During the welding process, the material flow velocity around the tool pin is higher in at the tool root than at the tool tip. Also, this velocity is higher at the retreating side than at the advancing side.
- At the beginning of the linear welding stage, the material is intensively heated and the heat is taken away (dissipated) slower than it is generated. Therefore, a decrease of heat generation rate is obtained. When the balance between the heat generation and dissipation is established, this rate becomes approximately constant.

Acknowledgement

The authors gratefully acknowledge the support from the Serbian Ministry of Education, Science and Technological Development under the projects TR 35002 and IP 451-03--2802/2013-16/69.

Nomenclature

A – material parameter of the Johnson-Cook model, [MPa]
A_5 – percentage elongation at fracture, [%]
B – material parameter of the Johnson-Cook model, [MPa]
C – material parameter of the Johnson-Cook model, [–]
c – specific heat capacity, [Jkg^{-1}°C^{-1}]
E – Young's modulus, [GPa]
h – heat convection coefficient, [Wm^{-2}°C^{-1}]
k – stiffness coefficient, [Nm^{-1}]
m – material parameter of the Johnson-Cook model, [–]
n_{rot} – rotation speed of the tool, [rpm]
n – material parameter of the Johnson-Cook model, [–]
p – body force, [N]
R_m – tensile strength, [MPa]
$R_{p0.2}$ – yield strength, [MPa]
T – temperature, [°C]
T_{melt} – solidus temperature, [°C]
T_{room} – ambient temperature, [°C]
t – time, [s]
u – displacement, [m]
v_{plunge} – plunging speed of the tool, [mms^{-1}]

Greek symbols

α – coefficient of thermal expansion, [°C^{-1}]
$\dot{\gamma}$ – slip rate, [mms^{-1}]
ε_p – equivalent plastic strain, [–]
$\dot{\varepsilon}_p$ – equivalent plastic strain rate, [s^{-1}]
$\dot{\varepsilon}_0$ – reference plastic strain rate, [s^{-1}]
ν – Poisson's ratio, [–]
ρ – density, [kg m^{-3}]
σ_y – current flow stress in the Johnson-Cook model, [MPa]

References

[1] ***, *Specification for Friction Stir Welding of Aluminum Alloys for Aerospace Hardware*, American National Standard, AWS D17.3/D17.3M:2010, American Welding Society, Miami, Fla., USA, 2010
[2] Park, K., Development and Analysis of Ultrasonic Assisted Friction Stir Welding Process, Ph. D. thesis, University of Michigan, Ann Arbor, Mich., USA, 2009
[3] Veljić, D. *et al.*, Numerical Simulation of the Plunge Stage in Friction Stir Welding, *Structural Integrity and Life, 11* (2011), 2, pp. 131-134
[4] Veljić, D. *et al.*, A Coupled Thermo-Mechanical Model of Friction Stir Welding, *Thermal Science, 16* (2012), 2, pp. 527-534
[5] Veljić, D. *et al.*, Heat Generation during Plunge Stage in Friction Stir Welding, *Thermal Science, 17* (2013), 2, pp. 489-496
[6] Feulvarch, E. *et al.,* A Simple and Robust Moving Mesh Technique for the Finite Element Simulation of Friction Stir Welding, *Journal of Computational and Applied Mathematics*, *246* (2013), pp. 269-277
[7] Song, M., Kovačević, R., Numerical and Experimental Study of the Heat Transfer Process in Friction Stir Welding, *Journal of Engineering Manufacture*, *217* (2003), 1, pp. 73-85
[8] Chen, C. M., Kovačević, R., Finite Element Modelling of Friction Stir Welding – Thermal and Thermomechanical Analysis, *International Journal of Machine Tools & Manufacture*, *43* (2003), 13, pp. 1319-1326
[9] Eramah, A. *et al.*, Influence of Friction Stir Welding Parameters on Properties of 2024 T3 Aluminium Alloy Joints, *Thermal Science, 17* (2013), Suppl. 1, pp. 21-27
[10] Mijajlović, M. *et al.*, Experimental Studies of Parameters Affecting the Heat Generation in Friction Stir Welding Process, *Thermal Science, 16* (2012), Suppl. 2, pp. 351-362
[11] Eramah, A. *et al.*, Impact Fracture Response of Friction Stir Welded Al-Mg Alloy, *Structural Integrity and Life, 13* (2013), 3, pp. 171-177
[12] Schmidt, H., Hattel, J., A Local Model for the Thermomechanical Conditions in Friction Stir Welding, *Modelling & Simulation in Materials Science and Engineering,13* (2005), 1, pp. 77-93
[13] Zhang, Z. *et al.*, Effect of Traverse/Rotational Speed on Material Deformations and Temperature Distributions in Friction Stir Welding, *Journal of Materials Science & Technology, 24* (2008), 6, pp. 907-913
[14] Veljić, D. *et al.*, Experimental and Numerical Thermo-Mechanical Analysis of Friction Stir Welding of High-Strength Aluminum Alloy, *Thermal Science, 17* (2013), Suppl. 1, pp. S28-S37
[15] Živojinović, D. *et al.*, Crack Growth Analysis in Friction Stir Welded Joint Zones using Extended Finite Element Method, *Structural Integrity and Life, 13* (2013), 3, pp. 179-188
[16] ***, *Approved Certificate of Conformity No. 47831*, ALCOA International, Inc., New York, USA

[17] ***, ASM International Aluminum 2024-T351 Data Sheet, http://asm.matweb.com/search/SpecificMaterial.asp?bassnum=MA2024T351
[18] Ivanović, I. *et al.*, Numerical Study of Transient Three-Dimensional Heat Conduction Problem with a Moving Heat Source, *Thermal Science, 15* (2011), 1, pp. 257-266
[19] Berković, M. *et al.*, Analysis of Welded Joints by Applying the Finite Element Method, *Structural Integrity and Life, 4* (2004), 2, pp. 75-83
[20] Aburuga, T. *et al.*, Numerical Aspects for Efficient Welding Computational Mechanics, *Thermal Science, 18* (2014), Suppl. 1, pp. S139-S148
[21] Mladenović, V. *et al.*, Numerical Analysis of Thermal Stresses in Welded Joints Made of Steels X20 and X22. *Thermal Science, 18* (2014), 1, pp. 121-126
[22] Rakin, M. *et al.*, Modelling of Ductile Fracture Initiation in Strength Mismatched Welded Joint, *Engineering Fracture Mechanics, 75* (2008), 11, pp. 3499-3510
[23] ***, *Abaqus Analysis Manual*, Dassault Systemes, Paris, 2014
[24] Johnson, G. R., Cook, W. H., A Constitutive Model and Data for Metals Subjected to Large Strains, High Rates and High Temperatures, *Proceedings,* 7th International Symposium on Ballistics. The Hague, The Netherlands, 1983, pp. 541-547
[25] Lesuer, D. R., Experimental Investigations of Material Models for Ti-6Al-4V Titanium and 2024-T3 Aluminium, Final Report, Department of Transportation, Washington DC, USA, 2000

Paper submitted: September 4, 2015
Paper revised: December 11, 2015
Paper accepted: December 20, 2015